Self-Powered and Self-Healable Extraocular-Muscle-Like Actuator Based on Dielectric Elastomer Actuator and Triboelectric Nanogenerator

Yanze Liu[1,2], Shangzhi Yue[1], Zhongyuan Tian[1], Zijuan Zhu[2], Yongji Li[2], Xiangyu Chen[4], Zhong Lin Wang[3,4*], Zhong-Zhen Yu[1*], Dan Yang[1,2*]

[1]State Key Laboratory of Organic-Inorganic Composites, College of Materials Science and Engineering, Beijing University of Chemical Technology, Beijing 100029, China

[2]Beijing Key Laboratory of Advanced Functional Polymer Composites, Beijing University of Chemical Technology, Beijing 100029, China

[3]College of Materials Science and Engineering, Georgia Institute of Technology, GA, 30332 USA

[4]Beijing Institute of Nanoenergy and Nanosystems, Chinese Academy of Sciences, Beijing 101400, China

*E-mails: zlwang@gatech.edu (Z. L. Wang); yuzz@mail.buct.edu.cn (Z.-Z. Yu); danyang@buct.edu.cn (D. Yang)

This article has been accepted for publication and undergone full peer review but has not been through the copyediting, typesetting, pagination and proofreading process, which may lead to differences between this version and the Version of Record. Please cite this article as doi: 10.1002/adma.202309893.

ABSTRACT: Although dielectric elastomer actuators (DEAs) are promising artificial muscles for use as visual prostheses in patients with permanent oculomotor nerve palsy (ONP), high driving voltage coupled with the vulnerable compliant electrodes coated on the dielectric elastomers limits their safe long-term service. Herein, a self-healable polydimethylsiloxane compliant electrode based on reversible imine bonds and hydrogen bonds was prepared and coated on both sides of an acrylic ester film to develop a self-healable DEA (SDEA), followed by actuation with a high-output triboelectric nanogenerator (TENG) to construct a self-powered DEA (TENG-SDEA). Under 135.9 kV/mm, the self-powered SDEA exhibited an elevated actuated strain of 50.6%, comparable to the actuation of SDEA under DC power. Moreover, the mechanically damaged TENG-SDEA displayed a high self-healing efficiency of over 90% after self-healing for 3 h at room temperature for 10 cycles. A low electric current of TENG ensuring the safe using of TENG-SDEAs and an extraocular-muscle-like actuator with oriented motion ability integrated by several TENG-SDEAs was constructed. Additionally, the SDEA was directly used as a flexible capacitive sensor for real-time monitoring of the patient's muscle movement. Accordingly, a medical aid system based on a conjunction of the extraocular-muscle-like actuator and flexible capacitive sensor was manufactured to helped the patients suffering from permanent ONP with disease control and prevention, as well as serve in physical rehabilitation and treatment.

Keywords: dielectric elastomers; triboelectric nanogenerator; self-healable actuators; compliant electrodes; capacitive sensors

1. Introduction

Permanent oculomotor nerve palsy (ONP) is mainly caused by diseases, such as tumors, diabetes, and even head trauma.[1] The major consequence of ONP is a serious impairment of the eye movement, leading to a narrow field of view.[2] Therefore, the prostheses capable of assisting eye movement is required to yield the patients a wider view. However, rigid materials are commonly used for the preparation of prostheses. Also, the ill-fitting between the wearable prosthesis and the human body results in patients with extreme discomfort and even ulcers.[3] Dielectric elastomer actuators (DEAs) have been widely explored as artificial muscles. They consist of a dielectric elastomer film coated with compliant electrodes on both sides, able of converting electrical energy to mechanical energy. So far, DEAs have widely been applied in soft robots, artificial organs, and prostheses due to their large actuated strain, high energy density, and rapid response.[4] Especially, DEAs have the potential to be used in visual prostheses and remotely operated robotics by mimicking the working mechanism of human eyes.[5]

Unfortunately, DEAs often require DC power supplies to provide high driving voltages (about kV) for actuation, resulting in a great risk for the operators and devices.[6] Meantime, the consumption of fossil fuels is often needed to provide electrical energy by DC power, against sustainable development. Alternatively, triboelectric nanogenerators (TENGs) have received increasing attention as a green power generation technology due to their efficient

electromechanical conversion and high output voltage. More importantly, the extremely weak currents in TENGs result in safe operation as power supplies for daily motion monitoring sensors and clinical surgery.[7] In our previous study, a soft insulin pump based on the combination of DEAs and TENG was prepared to provide a safe therapy service for patients suffering from Diabetes Mellitus.[8] Nevertheless, the compliant electrodes playing the role of the outmost layers of DEAs are prone to mechanical damage under external stress.[9] Additionally, the defects formed in compliant electrodes during processing usually lead to a premature electric breakdown at lower voltages, inevitably shorting the safe long-term service of soft insulin pump.[10] Coincidentally, the crawling soft robot, tunable optical grating, and braille display system, which are all based on the combination of DEAs and TENG, are faced with the same problem of short service time brought by the compliant electrodes without self-healing ability.[11]

To deal with these problems, various compliant electrodes have been explored to self-clear by burning off the defects for ensuring the re-actuation of DEAs.[12] For example, Pei et al[10] prepared a self-clearing interpenetrating bilayer-compliant electrode by coating a thin layer of water-based polyurethane on a single-walled carbon nanotube layer. The water-based polyurethane layer acted as a dielectric barrier to suppress corona discharges from the nanotubes and effectively enhanced the self-clearing ability of the compliant electrode. In this way, the self-cleared DEA could be re-actuated to 170% actuated strain with

a self-healing efficiency of about 90%. However, mechanical damages, such as cracks and scratches on the self-clearing compliant electrodes can hardly be healed. Recent studies dealing with liquid dielectrics or liquid metal have demonstrated immediate self-healing of mechanical damage and electrical damage of DEAs through fluid transport.[13] For instance, a self-healable hydraulically amplified self-healing electrostatic (HASEL) actuator has been prepared based on the polydimethylsiloxane (PDMS) embedding with dielectric oils. After the electric breakdown, the dielectric oils immediately returned to an insulating state to allow the self-healing of HASEL from electric breakdown for 50 times.[13a] However, strict encapsulation is required to avoid liquid leakage in such DEAs.

Therefore, preparing compliant electrodes with intrinsic self-healing properties could prevent mechanical and electrical damage for prolonged lifetime service.[14] Self-healing can be achieved through reversible bonds, such as the Diels-Alder reaction, disulfide bonds, and oxime-carbamate bonds.[15] However, most self-healable polymers based on these reversible bonds require an external stimulus to complete the self-healing process. Besides, the complicated preparation process is disadvantageous for practical applications.

Imine bonds and hydrogen bonds have been widely used to prepare self-healing dielectric elastomers owing to their mild reaction conditions and excellent reconstruction ability without external stimulation.[16] Thus, preparing self-healable compliant electrodes

through reversible imine bonds and hydrogen bonds is simple and effective for preventing DEAs from mechanical and electric breakdowns.

Herein, self-healable compliant electrodes on the basis of reversible imine bonds and hydrogen bonds were fabricated by functionalization of carbon nanotubes (CNT) with polydopamine (PDA), and then followed by compounding with self-healable PDMS based on the reaction of amino-modified polydimethylsiloxane (PDMS-NH_2) and terephthalaldehyde (DFB). The as-obtained self-healable compliant electrodes were coated on both sides of an acrylic ester film to develop a self-healable DEA (SDEA), which was then further actuated by a high-output TENG to construct a self-powered DEA (TENG-SDEA). Afterward, an extraocular-muscle-like-based TENG-SDEA capable of assisting oriented eye movement along with a flexible capacitive sensor were prepared to construct a medical aid system, potential for disease prevention, as well as physical rehabilitation and treatment.

2. Results and discussion

The preparation process of self-healable PDMS-compliant electrodes and SDEA are illustrated in **Figure 1a**. The existence of hydrogen bonds between phenolic hydroxyl groups in CNT-PDA and amino groups in PDMS-NH_2 chains resulted in uniformly dispersed CNT-PDA in the PDMS matrix, conducive to excellent electrical conductivity.[17] In addition, the hydrogen bonds also provide the PDMS with a self-healing property. However, the

excellent self-healing property of PDMS is mainly derived from the imine bonds (C=N) formed between the amino groups in PDMS-NH_2 and the aldehyde groups in DFB.[18]

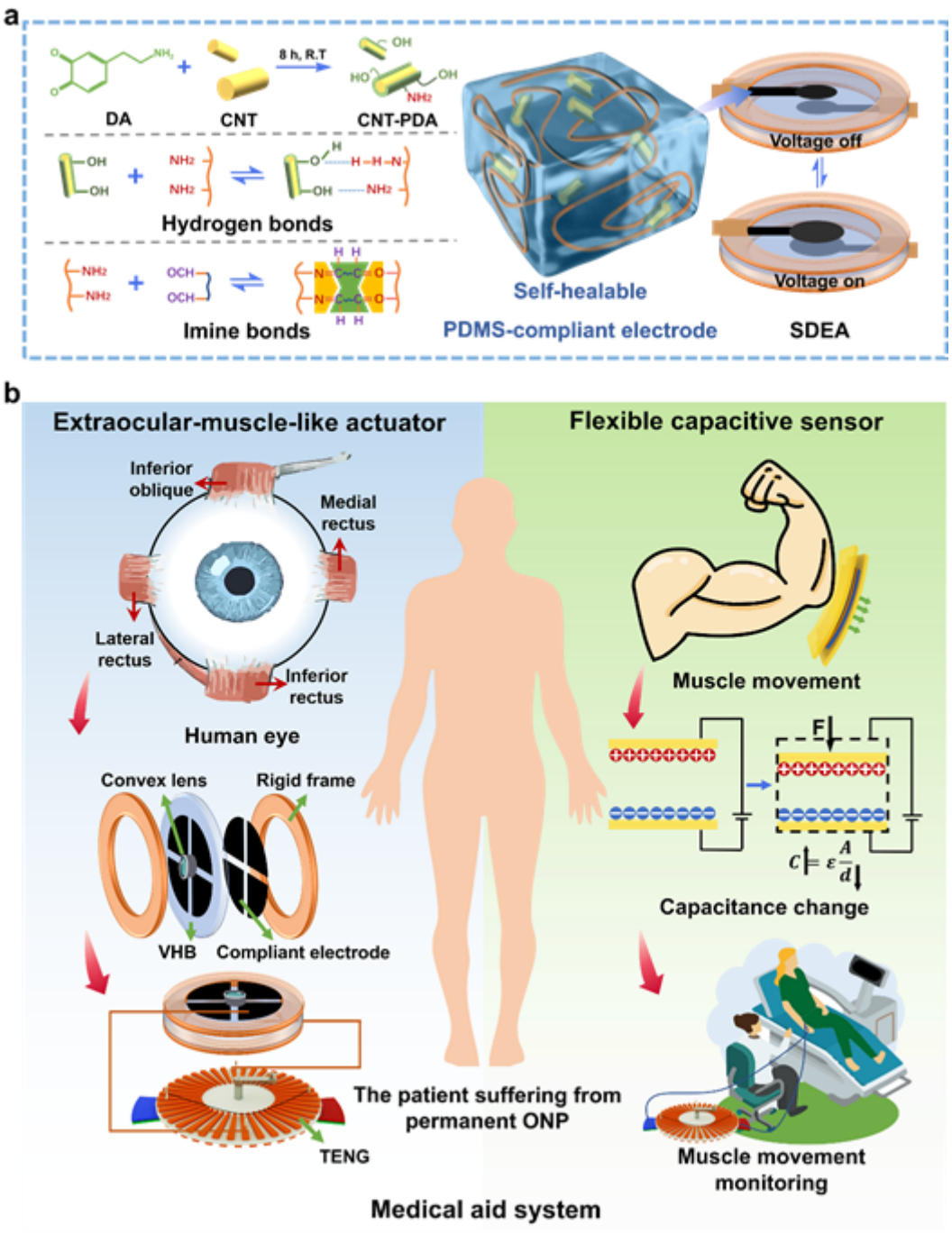

Figure 1. (a) The preparation process of self-healable PDMS-compliant electrodes and construction of SDEA. (b) A scheme of the medical aid system based self-powered extraocular-muscle-like actuator stimulating human eyes and a flexible capacitive sensor with real-time muscle movement monitor used for patients suffering from permanent ONP.

The corresponding dopamine self-polymerization mechanism[19] and photos of homogeneous dispersion of CNT-PDA in tetrahydrofuran (THF) are shown in **Figure S1** and **Figure S2**, respectively. The coating of the as-prepared self-healable PDMS-compliant electrode on the two sides of acrylate elastomer (VHB) film resulted in an SDEA, which then was further actuated by a high output TENG to construct a TENG-SDEA. A combination of several TENG-SDEAs resulted in a self-powered extraocular-muscle-like actuator stimulating human eyes, useful for assisting eye movement of patients suffering from OMP. On the other hand, the change in capacitance allowed the direct use of the SDEA as a flexible capacitive sensor capable of real-time monitoring of the patient's muscle movement. Accordingly, a medical aid system based on the extraocular-muscle-like actuator and the flexible capacitive sensor for patients suffering from permanent ONP was established (**Figure 1b)**.

The surface chemical compositions of CNT and CNT-PDA obtained from X-ray photoelectron spectroscopy (XPS) are depicted in **Figure S3**. Compared to pristine CNT, a new N peak (400 eV) appeared in the XPS wide scan spectrum of CNT-PDA, attributed to

the nitrogen-containing species in PDA. In addition, the N 1s spectrum can be curve-fitted into two peaks at 398.5 and 399.5 eV, assigned to the imine (=N-) and amine (-N-H) species in PDA, respectively. Comparison of the C 1s spectra between CNT and CNT-PDA revealed two new peaks at 286.4 eV and 288.9 eV, assigned to C-N and O-C=O species in PDA, respectively.[19a] The presence of C-N, O-C=O species, and N element proves successfully deposited PDA on the CNT surface.

The micromorphologies of CNT and CNT-PDA were studied by high-resolution transmission electron microscopy (HR-TEM) and the images are displayed in **Figure 2a** and **Figure S4**, respectively. Notably, a thin PDA layer with a thickness of about 1.1 nm was coated on the CNT surface. According to the X-ray diffraction (XRD) spectra **(Figure 2b)**, the PDA existed in amorphous form instead of crystalline form since no difference between the XRD spectrum of CNT and CNT-PDA was observed.[20] The grafting content of PDA is determined on the basis of the thermogravimetric analysis (TGA) results of CNT, PDA, and CNT-PDA (**Figure 2c)**. As the mass losses of CNT and PDA are respectively 5.17 and 50.03 wt% at 800 ^{o}C, the grafting rate of PDA is calculated as 23.73 wt%.

The successful synthesis of the PDMS-compliant electrode was further confirmed by fourier transform infrared (FT-IR) spectroscopy. In **Figure S5**, the new absorption peak at 1632 cm^{-1} in the PDMS matrix (PDMS-DFB) can be assigned to the stretching vibration of C=N of imine bonds, indicating successfully formed imine bonds by the reaction between

aldehyde groups in DFB and amino groups in PDMS-NH_2. Moreover, the hydrogen bonds formed between CNT-PDA and the PDMS matrix resulted in uniformly dispersed CNT-PDA in the PDMS matrix without serious agglomerations and good compatibility with the PDMS matrix (**Figure S6**). As shown in **Figure 2d-h,** the PDMS-compliant electrode exhibited favorable self-healing feature. The heart-shaped PDMS-compliant electrode was cut off by a sharp blade and the cut two pieces could be easily lifted against gravity after self-healing at room temperature for 30 s (**Figure 2d)**. Under optical microscopy (**Figure 2e**), the crack in the PDMS-compliant electrode completely vanished after self-healing. In addition, the PDMS-compliant electrode can be used as a wire in a conductive loop with an LED bulb. As depicted in **Figure 2f**, two pieces of cut PDMS-compliant electrode were connected to light the LED bulb again.

As good flexibility of compliant electrodes is also a prerequisite for DEA with large actuated strains,[21] the flexibility of PDMS-compliant electrodes was tested by the tensile stress-strain curves of PDMS-compliant electrodes with different CNT-PDA contents (**Figure 2g-h**). An elongation at a break of over 150% was obtained with the original and self-healed PDMS-compliant electrodes at CNT-PDA content of 5.0 wt%. The calculations based on elongation at break indicated self-healing efficiency reaching 95.1% using the PDMS-compliant electrodes with 5.0 wt% CNT-PDA (**Figure S7)**. Note that the elongation at the break of original PDMS-compliant electrodes declined as a function of the increase in

CNT-PDA content. Similar trend was observed in the stress-strain curves of the self-healed PDMS-compliant electrodes after mechanical damage (**Figure 2h)**. The decreased elongation at break can be ascribed to the declined slippage of polymer chains by adding more rigid CNT-PDA. Also, the incorporated rigid CNT-PDA declined the self-healing efficiency of PDMS-compliant electrodes due to the invalid reformation of imine bonds and hydrogen bonds.[22] Additionally, the flexibility of PDMS-compliant electrode was demonstrated by being twisted, bent, and wrapped on a glass rod, as shown in **Figure S8**.

The antibacterial property is another important performance feature for medical electronic devices, especially for ophthalmic devices. It has been discovered that the CNT shows antimicrobial activity to bacterial cells by its photothermal property. The temperature of PDMS-compliant electrodes is rapidly increased upon near-infrared light irradiation, and the thermal has been confirmed to damage the cell membrane of bacteria.[23] As demonstrated in **Figure 2i**, the inhibition efficiency of *E. coli* bacteria by PDMS-compliant electrode reached 99.9%, showing the safe and hygienic application of SDEA in medical aid systems.

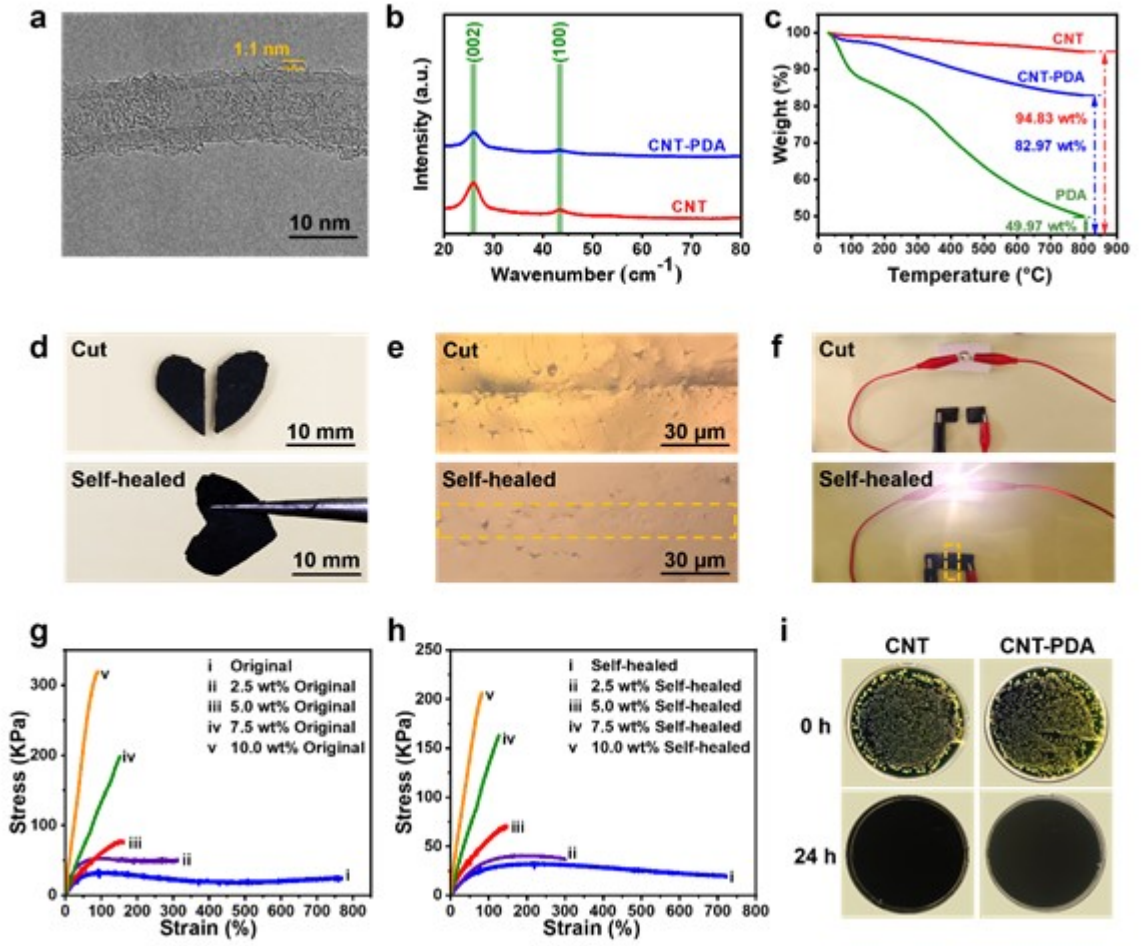

Figure 2. (a) HR-TEM image of CNT-PDA. (b) XRD spectra of CNT and CNT-PDA. (c) TGA curves of CNT, PDA, and CNT-PDA. Digital photos of (d) a heart-shaped compliant electrode being lifted after self-healing, (e) a self-healing process of a damaged PDMS-compliant electrode under an optical microscope, and (f) a PDMS-compliant electrode in a conductive loop with an LED bulb. Tensile stress-strain curves of PDMS-compliant electrodes with different CNT-PDA contents (g) before mechanical

damage and (h) after self-healing. (i) The *E. coli* colonies treated with PDMS-compliant electrodes after NIR irradiation.

The as-prepared PDMS-compliant electrodes were further coated on both sides of a VHB film to construct a SDEA. The actuation performances under DC driving are shown in **Figure 3a**. When the CNT-PDA content is lower than 2.5 wt%, no actuation was observed because of the ineffective electrically conductive paths in the PDMS-compliant electrodes. However, a maximum actuated strain of 52.3% was obtained by SDEA under 127.8 kV/mm at CNT-PDA content of 5.0 wt%. The addition of more CNT-PDA into the PDMS-compliant electrode resulted in a sharp decline in the maximum actuated strain of SDEA due to the increased rigidity of compliant electrodes. The self-healing efficiencies of SDEA based on dielectric strength and actuated strain were calculated and the results are given in **Figure 3e-f**. The self-healing efficiencies of the SDEA suffering from mechanical damage reached a maximum value of 98.3%, while actuated strains of SDEA suffering from electrical damage only recovered about 20% of their original values. This can be ascribed to the residual carbon and carbides in VHB caused by high temperature and high-energy charges will lead the VHB no longer remain insulated. Unfortunately, the residual carbon and carbides can hardly be removed conveniently.[24] Moreover, when PDMS-compliant electrode on the SDEA is applied with high electrical field, the electrical treeing caused by partial discharge of high voltage will induce pre-breakdown channels at defect sites and thus leads to damage caused

by electrical stress.[25] Additionally, a larger defect will be created due to the local heating and rapid vaporization of PDMS-compliant electrode during breakdown events.[26] Therefore, despite the good performance of SDEA in terms of actuation cycle stability even after self-healing from mechanical and electrical damage (**Figure 3g-i**), the unsatisfactory actuation performance of self-healed SDEA after electrical damage would limit the practical application as mentioned previously.[14a, 27]

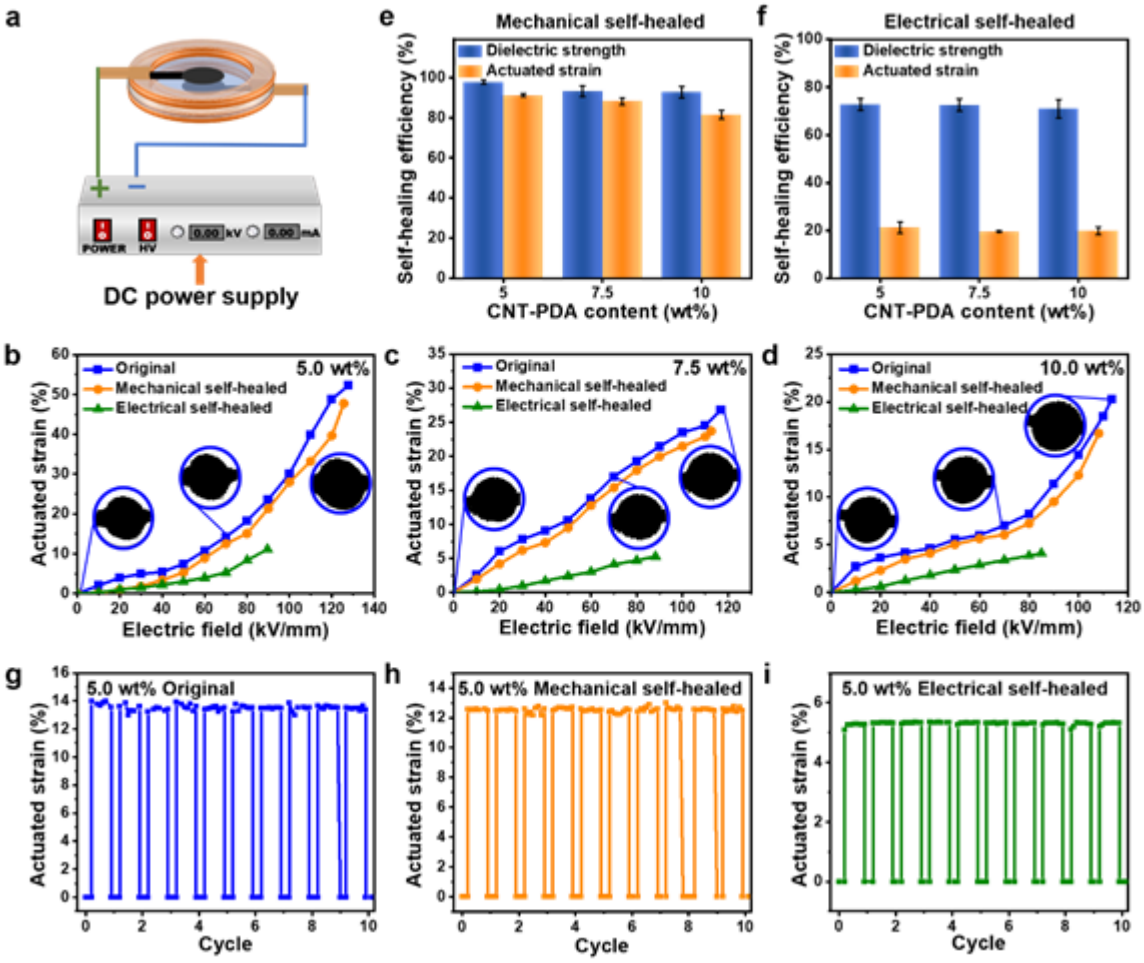

Figure 3. (a) Schematic diagram of SDEA under a DC power supply. The actuation performances of SDEA with (b) 5.0 wt%, (c) 7.5 wt%, and (d) 10.0 wt% CNT-PDA in compliant electrodes suffering from mechanical damage and electrical damage. Self-healing efficiency based on the maximum actuated strain and dielectric strength of SDEA under (e) mechanical damage and (f) electrical damages. Cycle stability on actuated strains of (g) original SDEA, (h) mechanical self-healed SDEA, and (i) electrical self-healed SDEA with 5.0 wt% CNT-PDA in compliant electrodes under 60 kV/mm.

As displayed in **Figure 3**, the high voltage provided by the DC power supply almost reached 120 kV/mm, a dangerous voltage value for humans and equipment. Thanks to the high output voltage (kV) and low output current (mA), TENGs can actuate SDEA in a safe and environmentally friendly manner.[28] The detailed structure of the high output voltage TENG in **Figure 4a** illustrated two fan-shaped blocks wrapped by triboelectric materials with opposite electrification polarity (Kapton and Nylon), a poly(methylmethacrylate) (PMMA) disk with two radially arrayed copper electrodes embedded, a transmission bridge with flexible wires connected the two opposite sides of the disk, and a pair of accumulators fixed vertically to the transmission bridge, and a handle to realize the rotation of the disk. The working mechanism of the high-output TENG can be divided into three steps. Firstly, the total charge of the electrode array on the top of the disk (transporting electrodes) was almost close to zero before contact with the transmission bridge. Secondly, the high electrostatic

field caused by the rotation of the disk resulted in charges with different polarities moving across the bridge, thus accumulating on the transporting electrodes. Under continuous rotation of the disk, more induced charges accumulated on the transporting electrodes. Finally, a high output voltage was established when the electrodes with induced charges were in full contact with the accumulator. Thus, a high output voltage can be achieved through the charge accumulation strategy by simply rotating the disk. In **Figure 4b**, a maximum value of 275 V was obtained for the TNEG, which is considered to be the voltage at which the air is broken down. By counting the number of LED lights lit, the maximum output voltage of TENG was calculated as 20 kV, indicating the TENG is able to directly actuate the SDEA.[29] However, the maximum transferred charge amount of the TENG was just about 270 nC (**Figure 4c**). Thus, the charge transferred once an electric breakdown occurred can be rapidly consumed to provide a self-protection mechanism for SDEA.

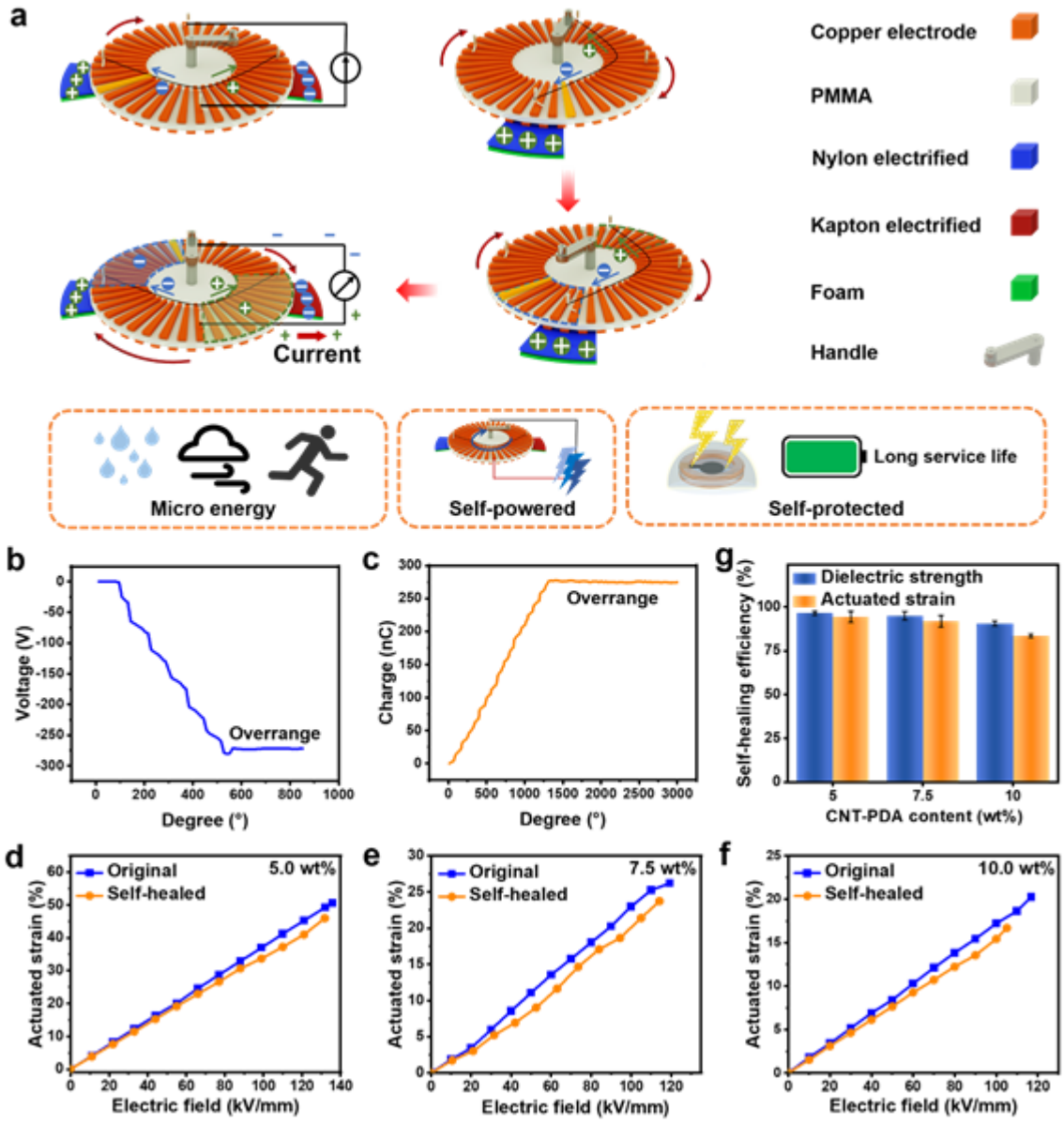

Figure 4. (a) Schematic diagram of the structure, working mechanism, and advantages of the high output TENG. (b) Open circuit voltage and (c) transferred charge amount of the high output TENG versus the rotation angle of the disk. The actuation performances of TENG-SDEA with (d) 5.0 wt%, (e) 7.5 wt%, and (f) 10.0 wt% CNT-PDA in the

PDMS-compliant electrode after mechanical damage. (g) Self-healing efficiency based on the maximum actuated strain and dielectric strength of TENG-SDEA after mechanical damage.

The actuation performance of the mechanical self-healed TENG-SDEA are provided in **Figure 4d-f**. Since no electric breakdown occurred, only mechanical damage was applied to TENG-SDEA. As the output voltage of TENG rose, the actuation strain of SDEA increased. However, the enhancement in CNT-PDA content declined the actuated strain and dielectric strength of TENG-SDEA. Under 135.9 kV/mm, the TENG-SDEA with 5.0 wt% CNT-PDA reached the maximum actuated strain of 50.6%, comparable to the actuation performance under a DC power supply. The calculated self-healing efficiencies based on the maximum actuated strain and dielectric strength of TENG-SDEA are summarized in **Figure 4g**. A high self-healing efficiency of 94.3% was obtained by the TENG-SDEA with 5.0 wt% CNT-PDA in the PDMS-compliant electrode, and the response and recovery times of TENG-SDEA is shown in **Figure S9**. Although it is well known that the VHB presents strong viscoelastic effects,[30] TENG-SDEA still exhibits relatively short response time (4 s) and recover time (16 s), much shorter than previous report (200 s and 250 s, respectively).[31] Moreover, the self-healing efficiency still maintained at 90% even after self-healing for 10 cycles (**Figure S10**). However, the self-healing efficiency showed an overall downward trend as a function of the increase in CNT-PDA content. Thus, the SDEA with 5.0 wt% CNT-PDA in the

PDMS-compliant electrode was used in subsequent applications due to its good actuation performance and excellent self-healing property.

An extraocular-muscle-like actuator-based TENG-SDEA capable of oriented moving was then prepared. As shown in **Figure 5a**, both sides of the four independent regions on VHB were coated with PDMS-compliant electrodes and connected to TENG, respectively. A convex lens was placed in the center of VHB to imitate the human lens. The center point of the convex lens was denoted A and the center point of the convex lens after actuation was named A'. The changes in displacement distance (denoted as 'd' in **Figure5b**) between point A and point A' versus the applied electric field are displayed in **Figure 5b** and **Figure S11**. Obviously, the changes in the visual field were not wide as human eyes since the retina would rotate together with the eyes, whereas the camera was fixed in front of the lens.[5a] Therefore, the displacement distance between point A and point A' only represented the planar movements of the soft lens. For example, the four compliant electrodes can be actuated independently to obtain different views (**Figure 5b.i),** with the maximum displacement distance reaching about 2.8 mm (**Figure S11)**. When a pair of electrodes on the same side was actuated (**Figure 5b.ii)**, the moving direction of the lens shifted from moving slanting upwards to moving straight upwards. Moreover, the displacement distance between A and A' in a self-healed extraocular-muscle-like actuator reached a self-healing efficiency of 88.2% after mechanical damage (**Figure 5b.iii** and **Figure S11)**. Therefore, the eyes of

patients suffering from ONP can move in eight directions with the aid of extraocular-muscle-like actuators.

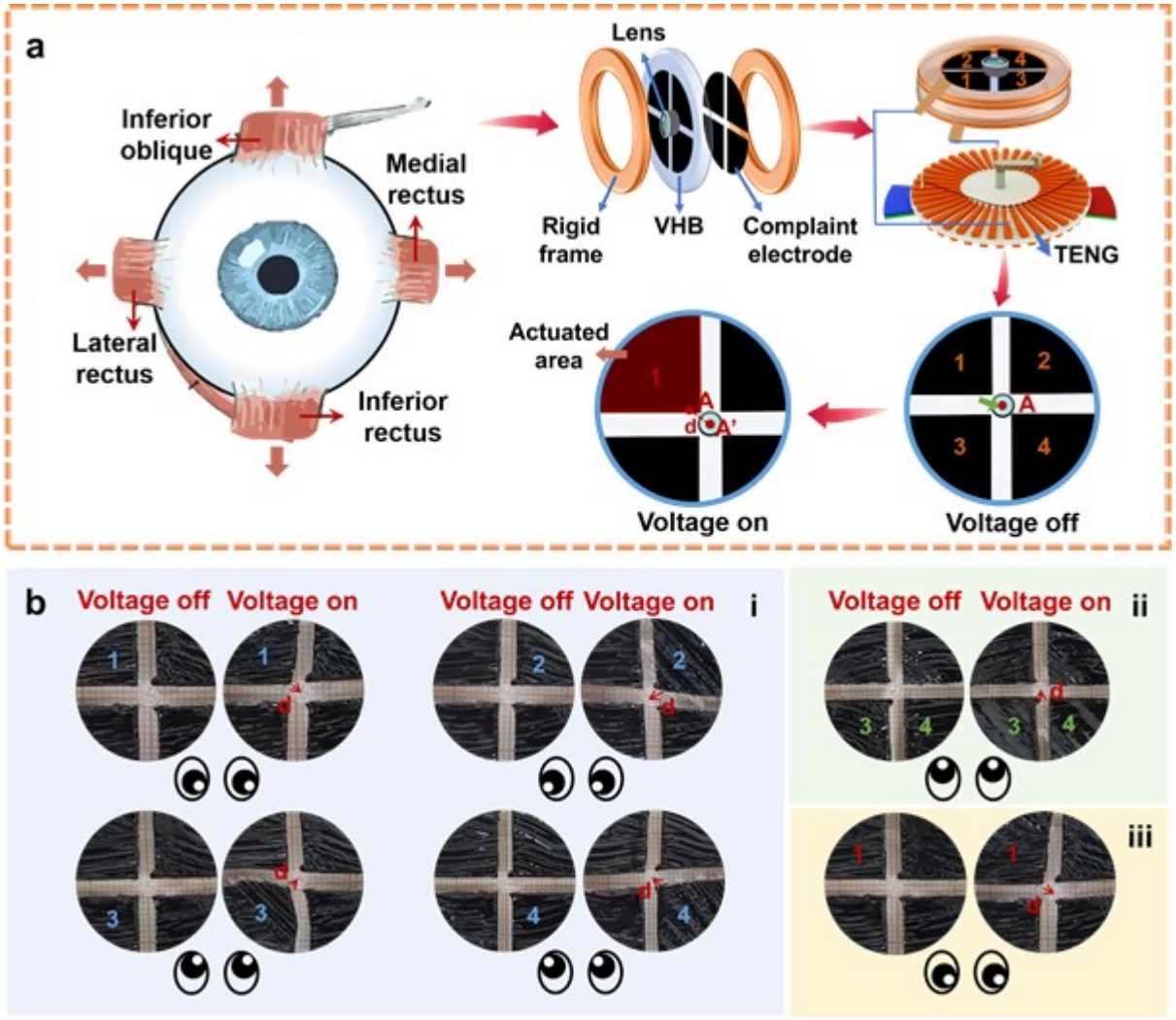

Figure 5. (a) The structure of extraocular-muscle-like actuator based on TENG-SDEA. (b) Images showing changes in extraocular-muscle-like actuator when actuated by (i) four independent compliant electrodes separately, (ii) two compliant electrodes on the same side,

and (iii) a self-healed compliant electrode. The compliant electrodes marked by numbers indicate an applied electrical field.

Although diabetes and head trauma may result in ONP, the amount of activity required by patients for the treatment of these two diseases is completely different.[32] Meanwhile, muscle motion monitoring is a simple method to track the rehabilitation degree of patients, which will improve the efficiency of health recovering. The as-prepared SDEA is also used as the flexible capacitive sensor for the real-time monitoring of patients suffering from ONP. The structure and the working mechanism of the flexible capacitive sensor are given in **Figure 6a**. The VHB was chosen to be the outmost layer of the flexile capacitive sensor due to its excellent sticky, considering that the PDMS-compliant electrode is unable to adhere directly to human skin. Besides, the outmost VHB provide support for the middle pre-stretched dielectric layer to acquire a large capacitance value. The classic plate capacitor calculation method ($C=\varepsilon_0\varepsilon_r S/d$) is suitable for the flexible capacitive sensor, where C, ε_0, ε_r, S, and d stand for the capacitance, vacuum permittivity, relative permittivity, plate area, and dielectric layer thickness, respectively. Under pressure or bending, the gauge factor of a flexible capacitive sensor (defined as $\Delta C/C_0$) would increase due to the decrease in distance between the two electrodes. Here, C_0 stands for the initial capacitance, while ΔC is the difference between the actual capacitance (C) and the initial capacitance. As shown in **Figure 6b-f** and **Video S9**, the flexible capacitive sensor responded sensitively and stably to continuous

motions, such as eye blinking, elbow bending, wrist bending, finger bending, and finger pressuring. The flexible capacitive sensor exhibited a response time of 0.38 s and a recovery time of 0.24 s, revealing a fast response (**Figure S12)**. However, $\Delta C/C_0$ during eye blinking gently (**Figure 6c**) and elbow bending (**Figure 6d**) was relatively small, which can be ascribed to the relatively small activity range and the relatively low pressure caused by the large joint area, respectively.[33] Furthermore, the flexible capacitive sensor exhibited excellent cyclic stability, as demonstrated by the stable $\Delta C/C_0$ during the loading-unloading pressing process for more than 5000 cycles (**Figure 6g**). The as-prepared flexible capacitive sensor with self-adhesion, rapid response, and high sensitivity looks very promising in real-time monitoring of muscle and eye movements in patients when combined with the Internet to form the interconnection between patients and machines.[34]

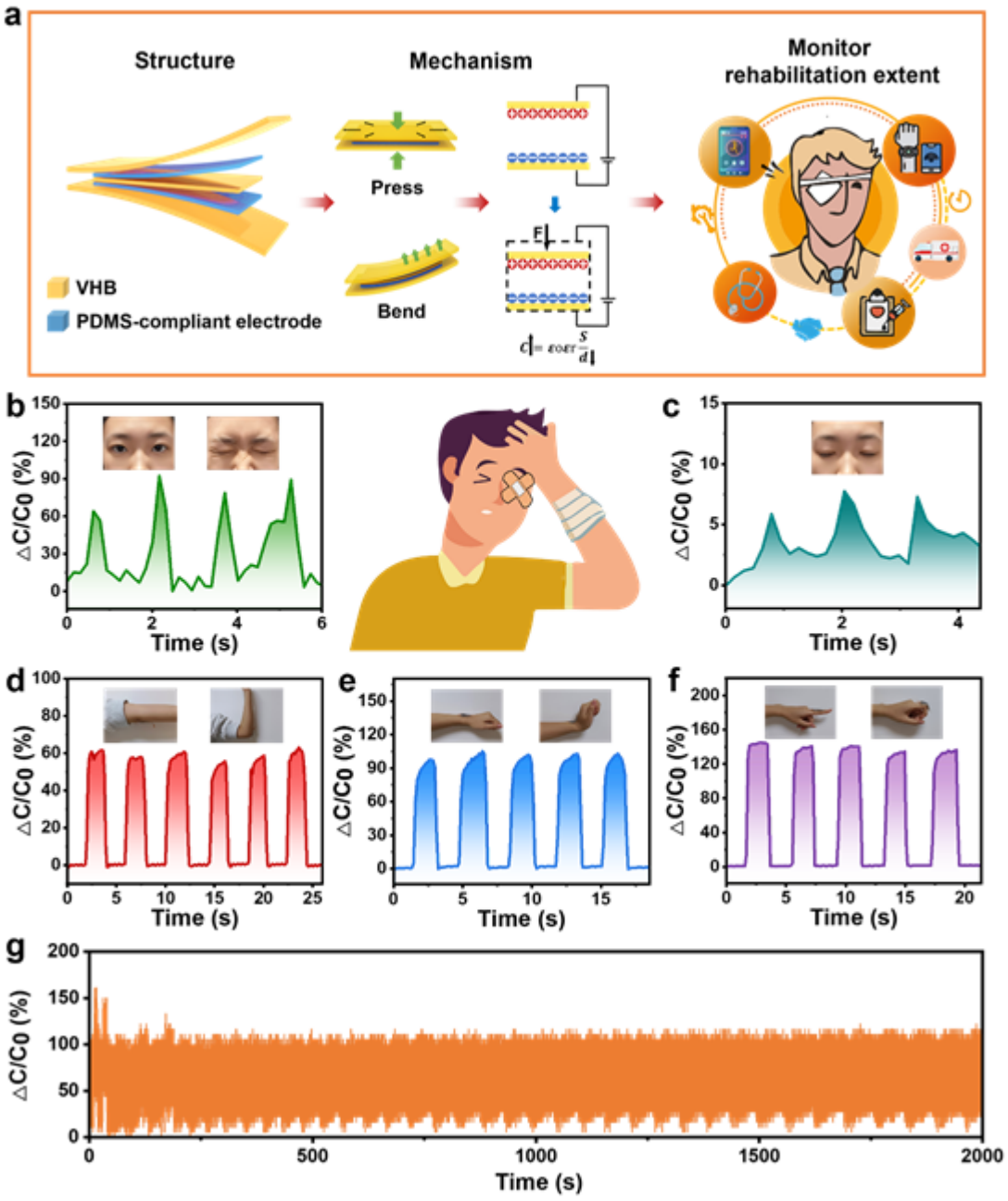

Figure 6. (a) Structure and working principle of the flexible capacitive sensor for real-time muscle movement monitoring. The $\Delta C/C_0$ of the flexible capacitive sensor during (b) eye blinking heavily, (c) eye blinking gently, (d) elbow bending, (e) wrist bending, and (f) finger

bending. (g) Plots of $\Delta C/C_0$ of the flexible capacitive sensor during loading-unloading pressing for 2000 s.

3. Conclusions

To prolong the service lifetime of DEAs as well as increase operational safety and durability, a self-healable PDMS-compliant electrode was successfully prepared using the reversible imine bonds and hydrogen bonds for developing an SDEA. Driven by a high output TENG, the self-powered DEA exhibited an elevated actuated strain of 50.6% under 135.9 kV/mm, comparable to the actuation of SDEA under DC power. Moreover, the mechanically damaged TENG-SDEA displayed a high self-healing efficiency of 94.3% after self-healing for 3 h at room temperature, and the self-healing efficiency still maintained at 90% even after self-healed for 10 cycles. The low electric current of TENG prevented electrical damage of TENG-SDEAs, thereby can safely be assembled as extraocular-muscle-like actuators to help patients suffering from ONP move their eyes in eight directions. Additionally, the SDEA can directly be used as a flexible capacitive sensor for real-time muscle movement monitoring when being squeezed or attached to various joints of the human body, and exhibited excellent cyclic stability for more than 5000 cycles. In sum, the safe, environmentally friendly, and conveniently actuated features of the proposed medical aid system based on the extraocular-muscle-like actuator and flexible capacitive sensor look promising for use in

disease control and prevention for patients suffering from permanent ONP, as well as in physical rehabilitation and treatment of other diseases.

4. Experimental section

4.1. Materials

Tris(hydroxymethyl)methyl aminomethane was obtained from Adamas (China). CNT was produced by Chengdu Organic Chemicals (China). PDMS-NH_2 (1400 mPa·s) was received from Guangzhou Xinguan Chemicals (China). VHB tape (acrylic foam tape), convex lens (d=3 mm), dopamine hydrochloride (DA), silicon oil (PMX-200), and DFB were all obtained from the local market.

4.2. Preparation of self-healable PDMS-compliant electrode

The process consisted of adding 1.5 g of DA and 3 g of CNT to 1.5 L of distilled water at pH 8.5 buffered by adding Tris. After mechanical stirring for 8 h under room temperature, the solution was filtered, washed with deionized water, and further dried to yield CNT-PDA. Next, different mass percentages of CNT-PDA (0, 2.5, 5.0, 7.5, and 10.0) were dispersed in 8 mL of THF under ultrasonic oscillation for 3 h. Afterward, 2.0 g of PDMS-NH_2, 0.2 g of silicone oil, and 4.5 mg of DFB were added and continuously stirred for 10 min. The mixture was then poured into a polytetrafluoroethylene mold and dried in a vacuum oven at 50 °C for 8 h to obtain the self-healable PDMS-compliant electrode.

4.3. Preparation of extraocular-muscle-like actuator and flexible capacitive sensor

First, a VHB film was pre-stretched to 400%. Four pieces of equal-size sector shape self-healable compliant electrodes were then coated on their two sides. Afterward, acrylic rigid frames were fixed to construct an extraocular-muscle-like actuation. Next, a convex lens was placed on the center of the as-prepared extraocular-muscle-like actuator to simulate the human retina. Here, the extraocular-muscle-like actuator was actuated by TENG to realize self-powering. On the other hand, the pre-stretched VHB film coated with equal-size self-healable compliant electrodes was directly used as a flexible capacitive sensor capable of detecting human muscle motions.

4.4. Characterization

Chemical compositions and structures of CNT and CNT-PDA were characterized by a Thermo Scientific Escalab 250Xi X-ray photoelectron spectroscopy (XPS) and a Labx XRD-6100 X-ray diffractometer (XRD). The surface micromorphology of CNT and CNT-PDA were observed by a Hitachi H9000 high-resolution transmission electron microscope (HR-TEM). Thermogravimetric analysis (TGA) was carried out on a TAQ5000 thermogravimetry analyzer under an argon atmosphere to determine the deposition content of PDA in CNT-PDA. A Bruker Invenio-S Fourier transform infrared (FT-IR) spectrometer was used to analyze the chemical structure of PDMS-compliant electrode. The cross-section fracture morphology of the PDMS-compliant electrode was observed on a ZEISS SUPRA55

scanning electron microscope (SEM). The mechanical damage and crack of the PDMS-compliant electrodes were produced by a sharp blade, and the self-healing process was observed using a Nikon E100 optical microscope. Mechanical property of the PDMS-compliant electrode was measured on a UTM-2460 universal testing machine at a crosshead speed of 5 mm/min. The antibacterial activity against *E. coli* ATCC 25922 was investigated *in vitro* using a spread plate method after the PDMS-compliant electrodes exposing to near-infrared light (808 nm) irradiation. The DC voltage was supplied by a Boer 71230 high-voltage power supply. After cutting and electric breakdown, self-healing tests of SDEA were carried out after self-healing for 3 h at room temperature. The changes in capacitance of the flexible capacitive sensor were recorded by a Keithley DAQ 6510. The self-healing efficiency is determined by the following formula:

$$H=\frac{S_O}{S_H}$$

where H is the self-healing efficiency, S_O is the original functional value of TENG-SDEA, and S_H is the functional value of self-healed TENG-SDEA, respectively. The displacement of the convex lens in the extraocular-muscle-like actuator is calculated by using the grid on the graph paper as the scale.

Statistical Analysis

All data were obtained from at least five independent samples and expressed as the mean ± standard deviation (with n = 5 per group).

Volunteer consent statement

The experiments involving human subjects were performed with the full consent of the participants and approved by the ethics committee of the Beijing University of Chemical Technology.

Supporting Information

Supporting Information is available from the Wiley Online Library or the corresponding author.

Figure S1. Self-polymerization of dopamine.

Figure S2. Images showing the dispersion of CNT and CNT-PDA in THF.

Figure S3. XPS wide scan, N 1s and C 1s spectra of CNT and CNT-PDA.

Figure S4. (a) Low- and (b) high-magnification TEM images of CNT.

Figure S5. FT-IR spectra of DFB, PDMS-NH_2, and PDMS-DFB.

Figure S6. SEM image of PDMS-compliant electrode with 5.0 wt% of CNT-PDA.

Figure S7. Self-healing efficiencies based on elongation at break of PDMS-compliant electrodes with different CNT-PDA contents.

Figure S8. The pictures of (a) twisted PDMS-compliant electrode, (b) bent PDMS-compliant electrode, and (c) PDMS-compliant electrode wrapped around the glass rod.

Figure S9. Response and recovery times of TENG-SDEA.

Figure S10. Self-healing efficiency of SDEA after 10 cycles of self-healing process.

Figure S11. Plots of displacement distance between A and A' versus applied electric field for (a) four independent compliant electrodes actuated separately, (b) two compliant electrodes on the same side actuated cooperatively, and (c) a self-healed compliant electrode actuated separately.

Figure S12. Response and recovery times of the flexible capacitive sensor.

Video S1. The mechanical self-healing ability of PDMS-compliant electrodes.

Video S2. The electrical self-healing ability of PDMS-compliant electrodes.

Video S3. Actuation performance of SDEA powered by DC power supply.

Video S4. Actuation performance of mechanical self-healed SDEA powered by DC power supply.

Video S5. Actuation performance of electrical self-healed SDEA powered by DC power supply.

Video S6. TENG-SDEA actuated in 5 cycles.

Video S7. Extraocular-muscle-like actuator powered by TENG.

Video S8. The flexible capacitive sensor responses to joint bending.

Video S9. The flexible capacitive sensor responses to finger pressing.

Declaration of Competing Interest

The authors declare that they have no known competing financial interests or personal relationships that could have appeared to influence the work reported in this paper.

Data Availability

Data will be made available on request.

Acknowledgements

Financial support from the National Natural Science Foundation of China (52273259) and the Fundamental Research Funds for the Central Universities (buctrc202217) are gratefully acknowledged.

References

[1] a)T. Kim, K. Nam, B. S. Kwon, Am J Phys Med Rehabil 2020, 99, 430; b)T. Suda, E. Matsushita, H. Minamide, QJM-INT J MED 2022, 115, 395; c)C. C. Chen, Br. J. Sports Med. 2005, 39, e34; d)T. Kim, K. Nam, B. S. Kwon, American Journal of Physical Medicine & Rehabilitation 2020, 99, 430;

[2] R. Kapoor, B. E. Kendall, M. J. Harrison, J. Neurol., Neurosurg. Psychiatry 1991, 54, 745.

[3] J. W. Kwak, M. Han, Z. Xie, H. U. Chung, J. Y. Lee, R. Avila, J. Yohay, X. Chen, C. Liang, M. Patel, I. Jung, J. Kim, M. Namkoong, K. Kwon, X. Guo, C. Ogle, D. Grande, D. Ryu, D. H. Kim, S. Madhvapathy, C. Liu, D. S. Yang, Y. Park, R. Caldwell, A. Banks, S. Xu, Y. Huang, S. Fatone, J. A. Rogers, Sci. Transl. Med. 2020, 12, eabc4327.

[4] a)J. Shintake, V. Cacucciolo, D. Floreano, H. Shea, Adv. Mater. 2018, 30, 1707035; b)R. Yin, D. Wang, S. Zhao, Z. Lou, G. Shen, Adv. Funct. Mater. 2020, 31, 2008936; c)A. Weymann, J. Foroughi, R. Vardanyan, P. P. Punjabi, B. Schmack, S. Aloko, G. M. Spinks, C. H. Wang, A. Arjomandi Rad, A. Ruhparwar, Adv. Mater. 2023, 35, 2207390; d)S. Xu, C. M. Nunez, M. Souri, R. J. Wood, Sci. Rob. 2023, 8, eadd4649; e)S. M. Mirvakili, I. W. Hunter, Adv. Mater. 2018, 30, 1704407; f)J. M. McCracken, B. R. Donovan, T. J. White, Adv. Mater. 2020, 32, 1906564.

[5] J. Li, Y. Wang, L. Liu, S. Xu, Y. Liu, J. Leng, S. Cai, Adv. Funct. Mater. 2019, 29, 1903762; b)S. Martin, A. Bruns, J. Franke, Adv. Funct. Mater. 2022, 32, 2112260.

[6] C. Zhang, B. Jin, X. Cao, Z. Chen, W. Miao, X. Yang, Y. Luo, T. Li, T. Xie, Adv. Mater. 2022, 34, 2206393.

[7] a)C. Wei, R. Cheng, C. Ning, X. Wei, X. Peng, T. Lv, F. Sheng, K. Dong, Z. L. Wang, Adv. Funct. Mater. 2023, 33, 2303562; b)F. Yi, Z. Zhang, Z. Kang, Q. Liao, Y. Zhang, Adv. Funct. Mater. 2019, 29, 1808849; c)H. Ryu, H.-m. Park, M.-K. Kim, B. Kim, H. S. Myoung, T. Y. Kim, H.-J. Yoon, S. S. Kwak, J. Kim, T. H. Hwang, E.-K. Choi, S.-W. Kim, Nat. Commun. 2021, 12, 4374; d)Y. Li, D. Yang, Z. Wu, F.-L. Gao, X.-Z. Gao, H.-Y. Zhao, X. Li, Z.-Z. Yu, Nano Energy 2023, 109, 108324; e)S. Si, C. Sun, Y. Wu, J. Li, H. Wang, Y. Lin, J. Yang, Z. L. Wang, Nano Res. 2023, doi:10.1007/s12274-023-6025-z; f)S. Yao, M. Zheng, Z. Wang, Y. Zhao, S. Wang, Z. Liu, Z. Li, Y. Guan, Z. L. Wang, L. Li, Adv. Mater. 2022, 34, 2205881; g)D. Yang, Y. Ni, X. Kong, S. Li, X. Chen, L. Zhang, Z. L. Wang, ACS Nano 2021, 15, 14653.

[8] Y. Wei, W. Wu, Y. Wang, X. Chen, Z. L. Wang, D. Yang, Adv. Funct. Mater. 2023, 33, 2213727.

[9] Z. Peng, Y. Shi, N. Chen, Y. Li, Q. Pei, Adv. Funct. Mater. 2021, 31, 2008321.

[10] W. Yuan, L. B. Hu, Z. B. Yu, T. Lam, J. Biggs, S. M. Ha, D. J. Xi, B. Chen, M. K. Senesky, G. Grüner, Q. Pei, Adv. Mater. 2008, 20, 621.

[11] a)W. Sun, B. Li, F. Zhang, C. Fang, Y. Lu, X. Gao, C. Cao, G. Chen, C. Zhang, Z. L. Wang, Nano Energy 2021, 85, 106012; b)X. Chen, Y. Wu, A. Yu, L. Xu, L. Zheng, Y. Liu, H. Li, Z. Lin Wang, Nano Energy 2017, 38, 91; c)X. Qu, X. Ma, B. Shi, H. Li, L. Zheng, C. Wang, Z. Liu, Y. Fan, X. Chen, Z. Li, Z. L. Wang, Adv. Funct. Mater. 2020, 31, 2006612.

[12] a)C. Baechler, S. Gardin, H. Abuhimd, G. Kovacs, Smart Mater. Struct. 2016, 25, 055009; b)S. Ahmed, Z. Ounaies, M. T. Lanagan, Smart Mater. Struct. 2017, 26, 105024.

[13] a)E. Acome, S. K. Mitchell, T. G. Morrissey, M. B. Emmett, C. Benjamin, M. King, M. Radakovitz, C. Keplinger, Science 2018, 359, 61; b)C. Pan, E. J. Markvicka, M. H. Malakooti, J. Yan, L. Hu, K. Matyjaszewski, C. Majidi, Adv. Mater. 2019, 31, 1900663; c)J. Xu, Y. Dong, Z. Jiang, L. Tang, X. Chen, Z. Yao, K. Cao, Composites, Part A 2021, 149, 106519; d)S. Li, M. Jiang, Y. Xie, H. Xu, J. Jia, J. Li, Adv. Mater. 2018, 30, 1706375.

[14] a)M. W. M. Tan, G. Thangavel, P. S. Lee, Adv. Funct. Mater. 2021, 31, 2103097; b)S. Bonardd, M. Nandi, J. I. Hernández García, B. Maiti, A. Abramov, D. Díaz Díaz, Chem. Rev. 2022, 123, 736.

[15] a)C. Choi, J. L. Self, Y. Okayama, A. E. Levi, M. Gerst, J. C. Speros, C. J. Hawker, J. Read de Alaniz, C. M. Bates, J. Am. Chem. Soc. 2021, 143, 9866; b)W. Yang, Y. Zhu, T.

Liu, D. Puglia, J. M. Kenny, P. Xu, R. Zhang, P. Ma, Adv. Funct. Mater. 2023, 33, 2213294; c)S. Yang, S. Wang, X. Du, Z. Du, X. Cheng, H. Wang, Chem. Eng. J. 2020, 391, 123544; d)W.-X. Liu, C. Zhang, H. Zhang, N. Zhao, Z.-X. Yu, J. Xu, J. Am. Chem. Soc. 2017, 139, 8678.

[16] a)J. Xu, J. Chen, Y. Zhang, T. Liu, J. Fu, Angew. Chem. Int. Ed. 2021, 60, 7947; b)H. Sun, X. Liu, S. Liu, B. Yu, N. Ning, M. Tian, L. Zhang, Chem. Eng. J. 2020, 384, 123242; c)Z. Yang, H. Li, C. Li, X. Lai, X. Zeng, Chem. Eng. J. 2022, 430, 133103.

[17] a)F. S. H. Simanjuntak, J. S. Choi, G. Lee, H. J. Lee, S. D. Lee, M. Cheong, H. S. Kim, H. Lee, Appl. Catal., B 2015, 165, 642; b)D. Yang, Y. Ni, X. Kong, H. Xue, W. Guo, L. Zhang, Appl. Surf. Sci. 2019, 495, 143638.

[18] B. Li, P.-F. Cao, T. Saito, A. P. Sokolov, Chem. Rev. 2022, 123, 701.

[19] a)W. Cheng, X. Zeng, H. Chen, Z. Li, W. Zeng, L. Mei, Y. Zhao, ACS Nano 2019, 13, 8537; b)Z. Jin, L. Yang, S. Shi, T. Wang, G. Duan, X. Liu, Y. Li, Adv. Funct. Mater. 2021, 31, 2103391.

[20] a)B. Chen, J. Li, M. Zhang, Z. Dong, K. Zhang, Composites, Part A 2022, 153, 106709; b)Y. Liu, W. Tu, M. Chen, L. Ma, B. Yang, Q. Liang, Y. Chen, Chem. Eng. J. 2018, 336, 263.

[21] R. Pelrine, R. Kornbluh, Q. Pei, J. Joseph, Science 2000, 287, 836.

[22] Y. Peng, H. Liu, H. Peng, J. Zhang, Matter 2023, 6, 226.

[23] a)Y. Hong, W. Shi, H. Wang, D. Ma, Y. Ren, Y. Wang, Q. Li, B. Gao, Environ. Sci.: Nano 2022, 9, 1000; b)G. Jiang, L. Chen, S. Zhang, H. Huang, ACS Appl. Mater. Interfaces 2018, 10, 36505; c)T. Mocan, C. T. Matea, T. Pop, O. Mosteanu, A. D. Buzoianu, S. Suciu, C. Puia, C. Zdrehus, C. Iancu, L. Mocan, Cell. Mol. Life Sci. 2017, 74, 3467.

[24] Y.-C. Zhang, W.-D. Li, X. Zhao, F.-B. Meng, P. Sun, C. Wang, G.-Z. Guo, W.-R. Li, G.-J. Zhang, Chem. Eng. J. 2023, 473, 145199.

[25] Y. Zhang, H. Khanbareh, J. Roscow, M. Pan, C. Bowen, C. Wan, Matter 2020, 3, 989.

[26] S. Hunt, T. G. McKay, I. A. Anderson, Appl. Phys. Lett. 2014, 104, 113701.

[27] a)M. W. M. Tan, H. Bark, G. Thangavel, X. Gong, P. S. Lee, Nat. Commun. 2022, 13, 6769; b)Y. Zhang, C. Ellingford, R. Zhang, J. Roscow, M. Hopkins, P. Keogh, T. McNally, C. Bowen, C. Wan, Adv. Funct. Mater. 2019, 29, 1808431.

[28] a)W. Sun, B. Li, F. Zhang, C. Fang, Y. Lu, X. Gao, C. Cao, G. Chen, C. Zhang, Z. L. Wang, Nano Energy 2021, 85, 106012; b)D. Yang, Y. Ni, H. Su, Y. Shi, Q. Liu, X. Chen, D. He, Nano Energy 2021, 79, 105394; c)Y. Zhang, K. Fan, J. Zhu, S. Wu, S. Zhang, T. Cheng, Z. L. Wang, Nano Energy 2022, 104, 107867.

[29] R. Lei, Y. Shi, Y. Ding, J. Nie, S. Li, F. Wang, H. Zhai, X. Chen, Z. L. Wang, Energy Environ. Sci. 2020, 13, 2178.

[30] a)L.-J. Yin, Y. Zhao, J. Zhu, M. Yang, H. Zhao, J.-Y. Pei, S.-L. Zhong, Z.-M. Dang, Nat. Commun. 2021, 12, 4517; b)J. Huang, X. Zhang, R. Liu, Y. Ding, D. Guo, Nat. Commun. 2023, 14, 1483.

[31] Y. Bar-Cohen, X. Zhang, M. Wissler, B. Jaehne, R. Breonnimann, G. Kovacs, in Smart Structures and Materials 2004: Electroactive Polymer Actuators and Devices (EAPAD), 2004, 5385, 78.

[32] a)H. Li, M. H. Hastings, A. Rosenzweig, Circulation Research 2020, 127, 1401; b)S. P. D. Chrisman, JAMA Pediatrics 2019, 173, 315.

[33] J. Wen, J. Tang, H. Ning, N. Hu, Y. Zhu, Y. Gong, C. Xu, Q. Zhao, X. Jiang, X. Hu, L. Lei, D. Wu, T. Huang, Adv. Funct. Mater. 2021, 31, 2011176.

[34] D. Liu, B. Chen, J. An, C. Li, G. Liu, J. Shao, W. Tang, C. Zhang, Z. L. Wang, Nano Energy 2020, 73, 104819.

Table of contents

A medical aid system combining with a self-powered extraocular-muscle-like actuator and a flexible capacitive sensor was constructed based on a self-healable dielectric elastomer actuator and a triboelectric nanogenerator, making it promising for using in disease control and prevention for patients suffering from permanent oculomotor nerve palsy through assisting eye movement and monitoring muscle movement.